Antimicrobial propensity of ultrananocrystalline diamond films with embedded silver nanodroplets

Daniel Merker[a], Blagovesta Popova[b], Thomas Bergfeldt[c], Tobias Weingärtner[c], Gerhard H. Braus[b], Johann Peter Reithmaier[a], Cyril Popov[a,*]

[a] *Institute of Nanostructure Technologies and Analytics (INA), Center for Interdisciplinary Nanostructure Science and Technology, University of Kassel, Heinrich-Plett-Str. 40, 34132 Kassel, Germany*
[b] *Department of Molecular Microbiology and Genetics and Göttingen Center for Molecular Biosciences (GZMB), Institute for Microbiology and Genetics, Universität Göttingen, Grisebachstr. 8, 37077 Göttingen, Germany*
[c] *Karlsruhe Institute of Technology, Institute of Applied Materials – Applied Materials Physics (IAM-AWP), Karlsruhe Nano Micro Facility (KNMF), Hermann-von-Helmholtz-Platz 1, 76344 Eggenstein-Leopoldshafen, Germany*

ARTICLE INFO

Keywords:
Ultrananocrystalline diamond films
Silver nanodroplets
Antibacterial material

ABSTRACT

Ultrananocrystalline diamond (UNCD) layers exhibit excellent mechanical properties and combine chemical inertness with good biological compatibility. Therefore, UNCD is considered a promising material for coating of implants. In this work we present the preparation of thin UNCD films with embedded silver nanodroplets that provide antimicrobial property, addressing another important topic concerning implant surgery, namely the risk of a life threatening bacterial infection. UNCD layers were prepared by microwave plasma-assisted chemical vapor deposition on a silicon substrate. Afterwards, a thin film of silver was deposited on top and treated by rapid thermal annealing (RTA) leading to dewetting and formation of silver nanodroplets on the surface. A second UNCD deposition with a short duration between 5 and 30 min was applied for capping the silver nanodroplets with a thin layer. The sample surfaces were characterized after each step by atomic force microscopy and scanning electron microscopy. The composition of the final samples, including the depth of the incorporated Ag nanodroplets, was analyzed by Auger electron spectroscopy. The impact of the silver layer thickness and the RTA temperature on the nanodroplet morphology was investigated. It was found that after 10 min of capping deposition the silver particles were completely covered with UNCD. In order to study the release of silver ions, the UNCD/Ag/UNCD samples were submerged in deionized water for 7 days at 37 °C, followed by detection of the silver concentration in the aqueous samples by inductively coupled plasma mass spectrometry. The determined concentration was strongly dependent on the thickness of the capping UNCD layer, exhibiting the highest silver content for the sample with the thinnest capping layer. Thus, the UNCD layer thickness can be utilized to control the amount of Ag ions released into the surrounding environment. The antibacterial properties were investigated with bacterial assays of the Gram-negative *Escherichia coli* and Gram-positive *Bacillus subtilis* bacteria that were exposed to the samples. All silver containing samples showed significant antimicrobial propensity, whereas the different capping thicknesses affected the time-course dependent antibacterial efficiency.
Prime novelty: Thin UNCD films were provided with supreme antibacterial propensity by embedding of silver nanodroplets. The thickness of the UNCD capping layer was varied and its influence on the release of silver in water was investigated. The UNCD/Ag/UNCD samples showed significant and controlled by the capping thicknesses time-dependent antibacterial efficiency against Gram-negative *E. coli* and Gram-positive *B. subtilis* bacteria.

1. Introduction

The first materials of choice for surgical and dental implants nowadays are medical (surgical) stainless steels or titanium and especially its alloys, such as TiAl6V4 or Ti6Al7Nb [1 3]. This is due to the good mechanical strength and corrosion resistance combined with relatively low costs in the first case, and to the biocompatibility of Ti and its mechanical properties, especially the high strength to weight

* Corresponding author.
E-mail address: popov@ina.uni-kassel.de (C. Popov).

ratio, a high fatigue strength, and the fact that the elastic modulus is close to that of bone in the second case [4]. However, these materials suffer from a loss of resistance to crevice corrosion processes. Another problem is the release of toxic ions from the surfaces of these implants into the surrounding tissue, which are afterwards transported and ac cumulated by the organs [3,5]. One generally accepted solution of these problems is the coating of the implant with a thin film thus retaining the excellent properties of titanium alloys or medical steels but ren dering the surface appropriately. Such a film has to be biocompatible, with good adhesion to the implant, excellent mechanical properties and adjustable (chemical) surface properties. In view of the biocompat ibility, carbon based materials are a first choice as carbon is the basis of any biological system. Moreover, there is quite a number of carbon based films providing the required mechanical and surface properties, for example diamond like carbon and ultrananocrystalline diamond.

Diamond is a material with outstanding properties, such as high hardness, high stiffness, extreme chemical stability, and biocompat ibility to name but a few. Diamond thin films are especially attractive as an implant coating material because they show sublime friction beha vior, which is extremely decisive when the implant is under high stress (knee or hip replacements). Additionally, diamond films promote the adhesion of cells on the surface of the implant showing a superior biocompatibility in comparison to established implant materials, such as titanium and its alloys [6]. Thin diamond films can be prepared with a wide variety of crystallite sizes ranging from single crystalline over poly and nanocrystalline down to ultrananocrystalline films (UNCD) [7]. The latter have the advantage of combining almost all of the above mentioned outstanding properties with rather smooth surfaces without any sharp tips and edges [8] which would be detrimental to many applications in the biomedical field. All diamond films have shown to be biocompatible [9]. Nevertheless, up to now the number of papers on the use of diamond and especially of UNCD as coating for implants is somewhat limited [8 15]. On the other hand, from these papers it is evident that diamond, especially in nano or ultrananocrystalline form, is an excellent choice for the coating of both parts of an implant, the stem to be integrated and the active working part, leading likewise to improved osseointegration and implant performance. Furthermore, such coatings could be rendered antibacterial, e.g. by incorporation of silver, which will suppress any post operation inflammatory processes.

The beneficial impact of silver when used in surgical instruments or as material for prosthetics on wound recovery after surgery is known since the early 16th century. The reason for this effect of silver re mained obscured until further investigations in the late 19th century revealed that not the silver itself exhibits antibacterial properties but the released silver ions from the bulk are the active agents. Therefore, chemical compounds which release silver ions like silver nitrate solu tions are probably the first prescription antibacterial medicine in troduced in the late 19th century. The fear of silver poisoning, called argyria, and the discovery of safer antibiotics like penicillin lead easily to the replacement of silver ion releasing medicine after the second world war [16].

In recent years the extensive over and misuse of antibiotics to treat infections in humans or to greater extent to treat animals in agricultural enterprises is responsible for the increasing danger of multiple drug resistant (MDR) bacteria which are in the worst case resistant to all antibiotics (also called superbugs) [17]. In contrast, a resistance of bacteria against silver ions is not known. Even though silver is used as an antimicrobial material for centuries, the pathways of antimicrobial action are still not fully understood. Different studies found that silver ions cause damage to microbes by several pathways. The antimicrobial activity of silver ions is closely related to their affinity towards thiol groups, although other target sites for interaction are also possible. Silver ions bind to the thiol group containing amino acid cysteine and inhibit the vital functions of enzymes and proteins in the bacteria causing their death. This was experimentally demonstrated as the an timicrobial activity of silver ions in a silver nitrate solution was neutralized by the addition of compounds containing thiol groups, such as free cysteine amino acids or sodium thioglycolate. It was also shown that compounds containing sulfur, but not as thiol groups, e.g. cy stathionine, L methionine or taurine, did not exhibit a neutralizing ef fect on the antimicrobial abilities of silver ions, confirming their spe cific affinity to the thiol groups [18]. Another effect of silver ions is the disturbance of various transport mechanisms of ions, such as phosphate or potassium, in the bacteria [19]. Additionally, the Ag ions influence the growth of the bacteria being deposited as granules into the vacuoles and cell walls, and inhibit the cell division during proliferation. Bac teria influenced by silver are increased in size and show structural abnormalities [20]. Moreover, the silver ion is meddling with the bacterial deoxyribonucleic acid (DNA) causing the transformation of the DNA into condensed form which affects the ability to replicate [21]. Finally, it was shown that silver ions induce the generation of reactive oxygen species (ROS), mostly the superoxide radical O_2^-, which are damaging the bacteria directly. The antimicrobial activity was sig nificantly decreased in anaerobic conditions showing the strong de pendency on oxygen presence. It is suggested that most likely the im pairment of the enzymes in the respiratory chain by silver ions is responsible for the formation of the ROS [22]. This reveals that the antimicrobial properties of silver are based on many different path ways, making it unlikely for bacteria to adapt on these mechanisms. On the other hand, silver can have a harmful effect on human cells. Dif ferent studies found that a silver concentration of over 10 µg/ml can be toxic for human cells [23]. An inhibitory effect on bacteria was ob served at a concentration of 0.3 µg/ml and a biocidal effect at 2 20 µg/ml [24 26].

Silver has been already used as a coating or included into industrial, medical and domestic products to prevent the spreading of microbes [27]. One example of combining silver with established materials is the attachment of titanium dioxide nanotubes loaded with Ag particles from a silver nitrate solution on titanium which exhibited antimicrobial effects to *Staphylococcus aureus* but also some cytotoxicity to rat os teoblasts. The latter issue can be addressed by reducing the amount of the loaded silver particles by changing the parameters during the sample preparation [28]. Another example is the investigation of stainless steel implants, used for fracture management as nails and plates for bone fixation, coated with silver particles by electrodeposi tion from a silver nitrate solution, which showed an antimicrobial effect to *Pseudomonas aeruginosa* decreasing 13 fold the number of bacteria compared to the uncoated implants. These samples showed no toxicity towards human osteoblast cells [29].

The focus of the research on combining the sublime mechanical performance of carbon films and the antibacterial properties of silver is set on amorphous diamond like carbon (DLC) films doped with Ag. This task is quite challenging since the incorporation of silver into carbon films does provide antimicrobial abilities but also can have significant impact on the mechanical properties. For example, stainless steel (SS) substrates were coated with DLC films by plasma enhanced chemical vapor deposition (PECVD) where for every 25 nm DLC layer thickness silver colloidal solution was sprayed on the surface resulting in a DLC Ag layer system [30]. The antibacterial activity was confirmed against *E. coli* with the DLC Ag film killing 70% of the bacteria after 3 h com pared to pure DLC with around 30% and SS with 0%. The difference between the pure DLC and DLC Ag samples vanished after 24 h with both showing the same antibacterial efficiency of around 30% which suggested a saturation of the Ag release since the antibacterial effi ciency of the aqueous silver colloidal solution was increasing with time from 50% after 3 h to 95% after 24 h. The number of Ag layers did not affect the antibacterial performance which indicated that only the layer closest to the surface (covered with 25 nm of DLC) was responsible for the initially increased antibacterial effect of the DLC Ag film compared to pure DLC. The hardness of the DLC film decreased with increasing the Ag content from 19 20 GPa to 11 16 GPa accompanied by decrease of the compressive stress [30]. Another paper showed similar results for

Ag containing DLC films regarding the decreased hardness, elastic modulus, wettability, surface energy and corrosion resistance [31], whereas other papers report an increase in hardness with an Ag content over 13 at.% [32]. In a review paper where DLC was discussed as a promising material for biological implants this issue was addressed as well [33]. The reduction of the stress and hardness was caused by the bonding behavior of Ag in the DLC films revealed by XPS measure ments. Ag remained in a metallic state within the DLC matrix and did not bond to carbon causing lower hardness and reduced stress. Another topic featured in this review paper was the effect of Ti on the DLC matrix which reduced the hardness but on the other hand improved the adhesion between the coating and the substrate preventing delamina tion. This is especially important since titanium has good mechanical properties but inhibits the growth of osteoblasts and therefore the coating of Ti with DLC could improve the osseointegration of such an implant [33]. The adhesion of the coating to the substrate could be also improved by doping the DLC layer with chromium which was shown in a paper where Ti6Al4V and CoCrMo substrates were coated with DLC by a hybrid process combining pulsed laser deposition (PLD) and magnetron sputtering with a varied amount of Cr up to 7 at.%. The critical load determined with a scratch tester increased with increasing the amount of Cr present in the DLC layer from 14 N for pure DLC to 19 N for DLC with the highest Cr concentration for the titanium alloy substrate. The antibacterial properties were tested against *P. aeruginosa* and *S. aureus* showing no effect which was explained by the increasing hydrophobicity preventing bacteria to adhere to the DLC surface which is antibacterial to a certain degree itself [34]. Besides chromium silicon was extensively studied as a dopant for DLC with beneficial effects on the mechanical and biological performance. In the following study ti tanium alloy Ti6Al7Nb was coated with DLC doped with Ag and Si (DLC Si/Ag) in various concentrations by radio frequency plasma as sisted chemical vapor deposition (RF PACVD). The Si doping was achieved by adding hexamethylsiloxane to the gas phase during the deposition and the Ag doping was achieved by sputtering a silver target attached to the rf electrode [35]. The Si in DLC caused lower internal stress, higher thermal stability, superior mechanical and tribological properties and increased corrosion resistance. Furthermore, the biolo gical compatibility was improved with better adhesion and spreading for endothelial cells and enhanced osteoblast proliferation on DLC Si. The Ag incorporation in the films provided antimicrobial abilities but could also have undesired effects on the mechanical properties as shown above. It was found that Ag in DLC Si/Ag was predominantly present in conglomerates and chemically bonded to the DLC matrix by forming Si O Ag groups which improved the hardness and biocompat ibility of the samples. With increasing the Ag concentration, the Si concentration was reduced resulting in a lowered hardness, bio compatibility (tested against endothelial cells) and an increased anti bacterial efficiency (tested against *E. coli*). In summary, the sample with the lowest Ag and the highest Si concentrations combined the benefits of both doping elements in DLC most efficiently resulting in an overall improvement compared to pure DLC [35]. Another research group coated Ti6Al4V disks and silicon samples via Ag containing poly vinylpyrrolidone (PVP) sol gel deposition and consequent plasma im mersion ion implantation resulting in DLC films containing Ag particles of diverse sizes with a total concentration up to 5 at.% Ag [36]. Here, unintentionally, a cover layer of silicon dioxide was deposited with a thickness of around 10 and 35 nm. The antibacterial efficiency was confirmed against *S. sanguinis* with live/dead viability test showing clear dependency on the thickness of the covering layer. 10% of the bacteria were killed with a SiO_2 covering layer thickness of 35 nm and 90% with a cover thickness of 10 nm. The authors argued that the Ag^+ ions could migrate through a thin covering layer enfolding their anti bacterial abilities to the adhered bacteria [36]. In the following paper the authors coated medical grade SS with Ag doped DLC by hybrid radio frequency/magnetron sputtering plasma assisted chemical vapor deposition (RF/MS PACVD) [37]. The Ag doping was carried out with an ion implanter resulting in samples with a silver surface content of up to 9 at.%. The viability of endothelial and osteoblast cells was tested showing a slight decrease in the proliferation of these cells at higher Ag concentrations confirming the harmful potential of silver ions on eu karyotic cells. The same samples showed increased antibacterial effi ciency against *E. coli*. This was not surprising because the known pathways of antibacterial action of Ag could be also applicable for cells, capable to induce apoptosis. The mechanisms of uptake and transport of Ag in the cells and the pathway of action leading to cell death in case of eukaryotic cells remained rather unclear and the results in literature were too divergent which made it difficult to identify the differences in cell and bacterial Ag uptake. However, the impact of Ag was limited on the cells and much better pronounced on the bacteria which supported the research for the utilization of Ag containing carbon film [37]. A topic to address on this issue was the release of Ag into the surrounding tissue and its kinetics. For instance, it would be desirable that the re lease of silver is the highest directly after the surgery to support the wound healing by killing the invasive bacteria in the injured tissue surrounding the implant. Afterwards it should decline rapidly with the time in order to reduce the effect of Ag on the attaching cells leading to enhancement of the implant integration. In the following study medical grade Ti6Al4V was coated with DLC embedded with Ag particles via a three step method including wet chemical Ag particle formation in PVP, dip coating and polymer to DLC conversion by plasma immersion ion implantation [38]. The prepared films had Ag content between 0.9 and 9 at.% at the surface and were tested for their biocompatibility with mammalian endothelial, osteoblast and fibroblast like cells by mea suring e.g. the metabolic activity. The antibacterial efficiency was confirmed against *S. aureus* and *S. epidermidis*. Furthermore, the silver release kinetics in simulated body fluid (SBF) was investigated via ICP optical emission spectroscopy (ICP OES) over 10 days with 1 day in terval. The samples showed antibacterial abilities against both bacteria with *S. aureus* being more persistent but even the sample with the lowest Ag content was able to inhibit the growth of both bacteria ef ficiently. This was the case for adhered bacteria as well as for plank tonic bacteria indicating a sufficient release of Ag into the aqueous supernatant for an inhibitory effect. The results for biocompatibility showed an inhibition of mammalian cell growth correlating with the Ag content in the sample. The Ag release kinetics revealed the desired behavior with a burst of high Ag concentration at the first day and subsequent lower Ag release in the following days. Mammalian cells grown on the surfaces which were already in contact with the culture medium and therefore had released most of the Ag were not affected at all by the sample. This proved further that Ag was released fast and readily during the first initial hours after the contact of these samples with the aqueous phase afterwards rapidly decreasing to low values near the detection limit of the used equipment [38]. The Ag release kinetics was also highlighted in a recent paper where DLC Ag films were deposited on Ti by thermionic vacuum arc giving films with Ag concentrations of 4 and 6 at.% [39]. The release of Ag was investigated over 10 days in phosphate buffered saline (PBS) via ICP mass spectro metry (ICP MS) and showed a rapid increase of the Ag content in the initial 12 h, a saturation within 66 h and a plateau after 120 h which agreed with the before mentioned findings. The release kinetics can differ depending on the sizes of the Ag particles because the smaller particle sizes increase the amount of the surface atoms which have a higher tendency to dissolute. The antibacterial activity was here con firmed against *S. aureus* with efficiencies of 95% for the sample with the highest silver concentration compared to uncoated Ti with an efficiency of 15% [39].

To the best of our knowledge carbon layers with a crystalline dia mond phase have not been subject to experiments aiming to include silver particles into the layer to provide antibacterial properties. An approach to achieve antibacterial properties of crystalline diamond relies on coating of nanoneedles structured in silicon substrate with diamond, so called black diamond (bD). The nanostrucuted bD killed

the Gram negative *Escherichia coli* mechanically due to stretching and disruption of the cell membrane [40]. The major geometric factor for the antibacterial efficency was the areal density of the nanoneedles, not their length. In contrast, the Gram positive *Streptococcus gondolii* were unaffected by the nanostructured surfaces, probably due to their smaller size, thicker cell membrane and/or lack of motility.

Here we report on the preparation of ultrananocrystalline diamond (UNCD) films by microwave plasma assisted chemical vapor deposition with embedding of silver nanodroplets after heat induced dewetting of a thin silver layer and their subsequent capping with a second UNCD layer (UNCD/Ag/UNCD). The composition of the films was investigated by Auger electron spectroscopy (AES) and the release of silver from the samples in deionized water was measured by inductively coupled plasma mass spectrometry (ICP MS). Finally, the antimicrobial properties were adressed with assays of bacteria incubated with the samples.

2. Experimental

2.1. Deposition of UNCD films

3 inch silicon (100) wafers (CrysTec) were used as substrates. In order to remove the native silicon dioxide layer the substrates were submerged in a commercial buffered oxide etch solution (NH_4F:HF 7:1, JT Baker) for 35 s. After rinsing the substrate with deionized water and drying with nitrogen it was submerged in a seeding solution which was a 1:3 mixture of commercial seeding slurry *Opal seeds* (Adamas Nanotechnologies Inc.) and methanol, in an ultrasonic bath for 30 min. The substrate was cleaned afterwards ultrasonically in aceton and isopropanol for 90 s each. After drying in nitrogen flow the Si wafer was charged into a microwave plasma assisted chemical vapor deposition (MWCVD) reactor (ASTeX). The substrate was heated to 550 °C in vacuum over a periode of 1 h before the gas mixture of 17% methane diluted in nitrogen was introduced into the reaction chamber. The microwave plasma was ignited with a power of 800 W and the working pressure was stabilized at ca. 30 kPa. With a duration of 3 h and a deposition rate of 4 nm/min under the above condition, the thickness of the UNCD film was ca. 720 nm. After the deposition the wafer was cut into 1×1 cm^2 pieces for further processing.

2.2. Deposition of silver nanodroplets and their capping with UNCD

The UNCD samples were coated with a thin layer of silver with thickness of 3 nm, 5 nm or 10 nm by electron beam deposition (PLS 500, Pfeiffer) at a pressure of around 10^{-5} Pa. After that they were subjected to rapid thermal annealing (RTA, Xerion) at temperatures of 550 °C, 650 °C and 750 °C (hold temperatures, HT) for 10 min in nitrogen flow. Details about the RTA treatment regimes are given in Table 1 and Fig. 1. Finally, the samples were once again introduced into the MWCVD setup for deposition of the capping layer with varied duration of 5 min, 10 min, 15 min and 30 min at the same process parameters as for the first UNCD deposition. The workflow of the preparation of UNCD/Ag/UNCD samples is presented in Fig. 2.

Table 1
RTA regimes for dewetting of Ag layers (RT – room temperature, HT – hold temperature of 550 °C, 650 °C or 750 °C).

Step	Time [s]	Temperature [°C]	N_2 flow [sccm]
Hold	60	RT	30,000 (flow 1)
Heating	90	RT to HT	10,000 (flow 2)
Hold	600	HT	10,000 (flow 2)
Cooling	300	HT to RT	30,000 (flow 1)

2.3. Characterization of the UNCD and silver nanodroplet morphology

Scanning electron microscopy (SEM) and atomic force microscopy (AFM) were primarily applied to control the morphology of the samples after each process step. All SEM micrographs were taken with SEM S 4000 (Hitachi Ltd.) in secondary electron mode with an acceleration voltage of 10 keV at a pressure of around 10^{-5} Pa. For AFM imaging a DualscopeTM SPM 95 (DME Nanotechnologie GmbH) operated in tapping mode at ambient pressure was used and software Gwyddion (Version 2.48) was utilized for post processing of the images.

The differences in the morphology of the silver nanodroplets by variation of the silver layer thickness and RTA temperature were investigated by calculation of the statistical distribution of the average droplet height after grain detection from the AFM images with Gwyddion by the so called watershed method.

2.4. Composition of UNCD/Ag/UNCD films and silver release in aqueous samples

The atomic composition and the depth of incorporation of Ag nanodroplets after UNCD overgrowth with different durations were revealed by Auger electron spectroscopy (AES) (680 Xi Auger Nanoprobe, PHI). The electron beam acceleration during measurements was 10 keV at a pressure of around 10^{-8} Pa with a resulting beam current of 10 nA and a beam inclination of 60° to the sample surface plane. The depth profile was achieved by alternating measurement and sputtering with an argon ion beam accelerated with 2 keV at a pressure of around 10^{-7} Pa resulting in a beam current of 500 nA and a beam inclination of 45° to the surface. The sputtering steps were 1 min each, followed by analyses of the composition. The sputter rate for UNCD films with these AES setup and sputter parameters was determined with a 220 nm thick sample, measured with a profilometer XP 100 (Ambios Technology). The high sensitive surface profiler is capable to measure step heights from ca. 1 nm to 1.2 mm with step height repeatability of 0.1%. The sample was deposited under the above mentioned conditions but for shorter time (45 min). In order to prepere a step for profilometry photolithography was implemented after deposition of a gold mask (200 nm thickness) and subsequent lift off process. The step was etched in an oxygen plasma (1000 W ICP Power, 200 W rf power, 666 Pa working pressure and 10 sccm O_2 flow giving an etch rate of ca. 200 nm/min) until the Si substrate was reached.

Silver release in liquid phase was examined with an inductively coupled plasma mass spectrometer (ICP MS) 7500ce (Agilent) with a detection limit for silver of 0.3×10^{-4} µg/ml. For preparation of the samples, 1×1 cm^2 Ag/UNCD and UNCD/Ag/UNCD were submerged in 20 ml of deionized water for 7 days at a temperature of 37 °C. The water samples were analyzed by ICP MS to reveal the concentration of released silver; deionized water was used as a negative control. All measurements were made in duplicate.

2.5. Bacterial assays

The antibacterial properties of the UNCD/Ag/UNCD samples were tested using *Escherichia coli* ($K-12$) and *Bacillus subtilis* (NCIB 3610) as reference strains for Gram negative and Gram positive bacteria, respectively. *Bacillus subtilis* is commonly spread in the soil, whereas *Escherichia coli* is found in environment, food and intestine of mammals and is one of the most frequent causes of many common bacterial infections. The cells were grown overnight in Lysogeny broth (LB) medium at 35 °C and then diluted in sterile phosphate buffered saline (PBS) buffer to a concentration of 10^6 colony forming units (CFU)/ml. The tested layers (1×1 cm^2) were placed into 12 well culture plates and covered with 1 ml of the cell suspension. Pure bacterial culture was incubated in an empty well. The sterile chambers were incubated at 35 °C. After 3 h, 8 h and 24 h aliquots of 100 µl were taken. The cell aliquots were diluted down to 10^{-3} in PBS and 100 µl of the diluted cell

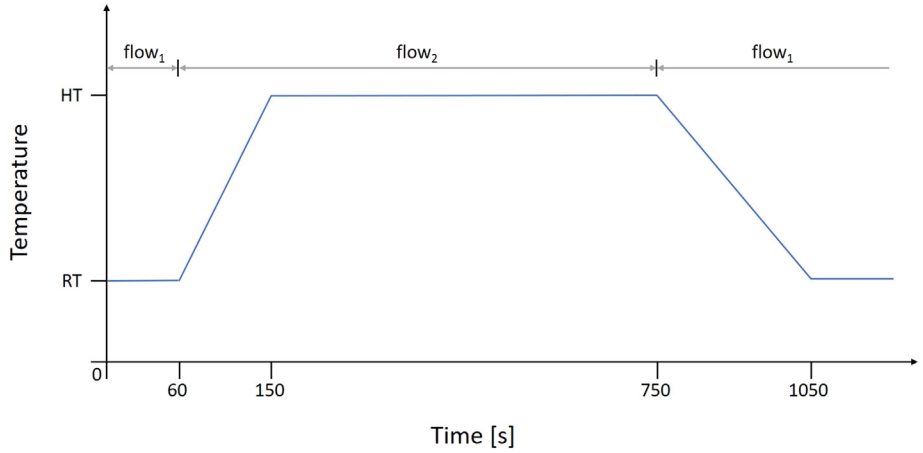

Fig. 1. RTA regime for dewetting of the thin Ag layers on top of UNCD and formation of Ag nanodroplets.

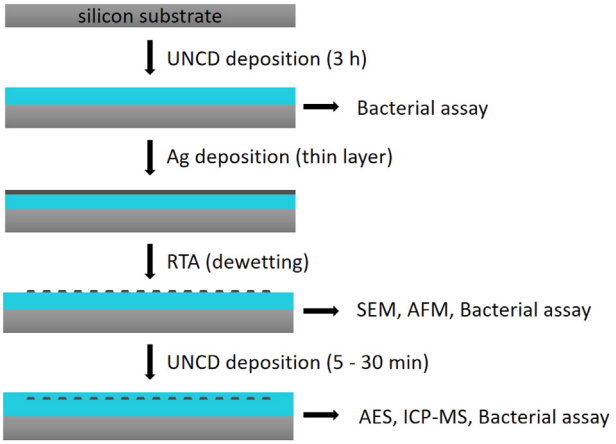

Fig. 2. Workflow of the preparation of UNCD/Ag/UNCD samples and their characterization.

suspension was spread over LB agar plates. The plates were incubated overnight at 35 °C and the number of CFU per plate was counted. All experiments were performed in triplicates.

3. Results and discussion

3.1. Basic properties of the UNCD films

The structural and electronic properties of the UNCD layers grown in the same setup under the same conditions were investigated in several previous studies, as summarized below. Transmission electron microscopy (TEM) revealed that the layers consisted of diamond crystallites with a diameter of up to 10 nm surrounded by a grain boundary with a width of 1 1.5 nm [41,42]. The volume ratio of crystalline and amorphous carbon was close to unity and the content of sp^2 carbon was in a range of 10 15% as studied by X ray photoelectron spectroscopy (XPS). Atomic force microscopy (AFM) showed that the surface topography was dominated by spherical features with a diameter of around 100 nm giving a rms roughness of 12 14 nm [43]. The incorporation of hydrogen in the UNCD films was investigated by nuclear reaction analysis (NRA) and Fourier transform infrared spectroscopy (FTIR). It was found that the hydrogen content in the bulk was 7.5 8 at.% predominantly bonded to sp^3 carbon and increasing towards the surface to around 14 at.% [44]. The content of nitrogen and oxygen was ca. 1 at.% in the bulk, the oxygen surface concentration was up to 4 at.%. Due to the hydrogen termination, the as grown UNCD layers exhibited p type surface conductivity with a sheet resistance of 0.14 Ω and a sheet carrier density of 7.6×10^{12} cm^{-2}. while the bulk conductivity was ca. seven orders of magnitude lower [45]. The contact angle of the as grown UNCD against water was around 70° [41].

3.2. Morphology and distribution of the silver nanodroplets

Initially, the dewetting process which lead to the formation of the silver nanodroplets was investigated. It utilizes the well known melting point depression by decreasing the size of the material in at least one dimension (thin film in our case) which increases the relative amount of more energetic surface atoms. The melting point can be decreased by several hundred degrees for a layer with thickness of a few nanometers. For the current study we tested three silver film thicknesses of 3 nm, 5 nm and 10 nm deposited ontop of the UNCD layers. Subsequently an extended heating step of 10 min at a selected temperature was carried out in the RTA setup for nanodroplet formation. The selected temperatures were 550 °C, 650 °C or 750 °C, chosen according to the the substrate temperature during the UNCD capping deposition: around 550 °C before the plasma was ignited and slightly higher afterward. Samples were prepared with different combinations of Ag layer thickness and annealing temparature, and examined with SEM.

All SEM micrographs showed the formation of silver nanodroplets on the UNCD surface after the RTA treatment (Fig. 3). With increasing the layer thickness, the size of the nanodroplets also increased, most pronounced in the SEM image of the sample with initial Ag layer thickness of 10 nm (Fig. 3 (c)). The difference in droplet size between the samples with 3 nm and 5 nm layer thicknesses was not so apparent (Fig. 3 (a) and (b)). Regarding the effect of the annealing temperature there were only minor differences between 550 °C and 650 °C as seen in the corresponding SEM micrographs (Fig. 4 (a) and (b)). On the other hand, the SEM micrograph from 750 °C treatment temperature differs significantly from the before mentioned. It seems like the uniformity of the nanodroplets was lost resulting in larger silver particles of diverse sizes and forms (Fig. 4 (c)).

The same samples were investigated by AFM in order to determine the size of the nanodroplets and their statistical distribution. The Ag layer with thickness of 3 nm resulted in the formation of silver nanodroplets with height of around 60 nm whereas nanodroplets of around 50 nm were formed from the thicker layer of 5 nm (Fig. 5 (a)). For the 10 nm layer thickness the results were in agreement with the SEM micrographs showing the largest nanodroplets with mean height of around 100 nm. Concerning the temperature dependency the results revealed clearly that the Gaussian like shape of the distribution curve was lost in case of RTA temperature of 750 °C indicating the loss of the uniformity of the nanodroplets (Fig. 5 (b)). In contrast, the curves for the annealing temperatures of 550 °C and 650 °C were similar indicating no or very small effect of the temperature in this range on the

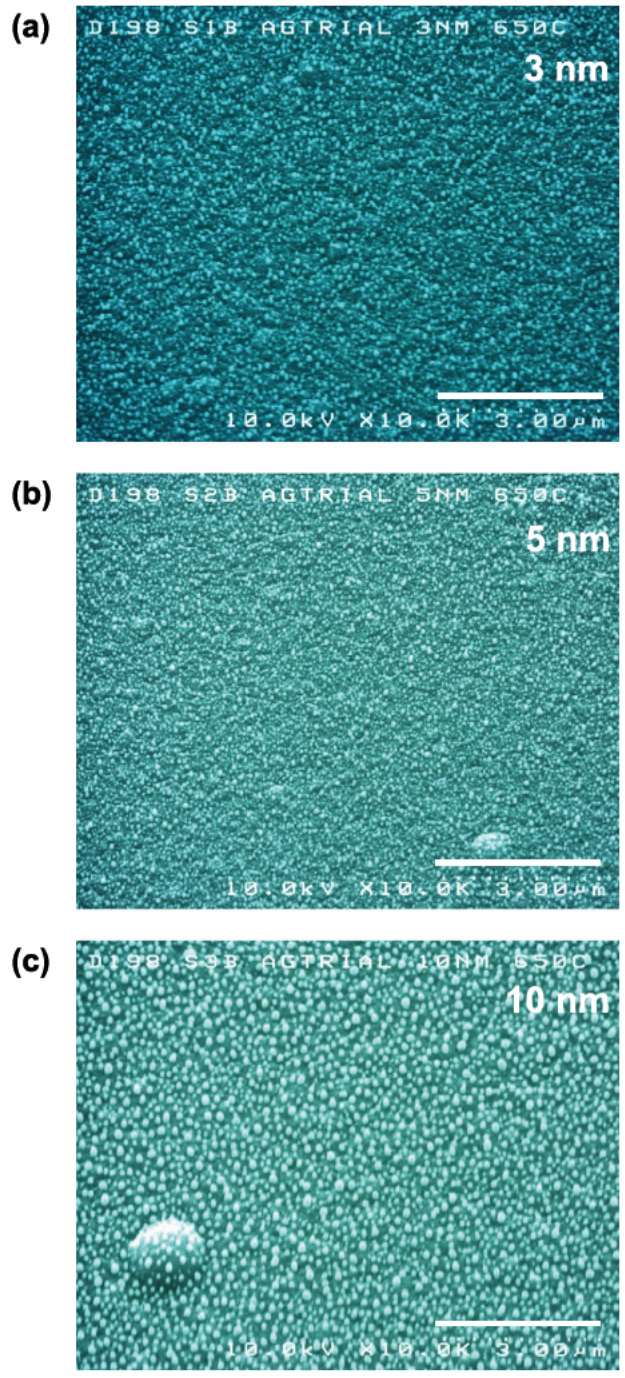

Fig. 3. SEM micrographs of silver nanodroplets obtained from different layer thicknesses (3 nm, 5 nm and 10 nm) after annealing at a temperature of 650 °C (marker 3 µm).

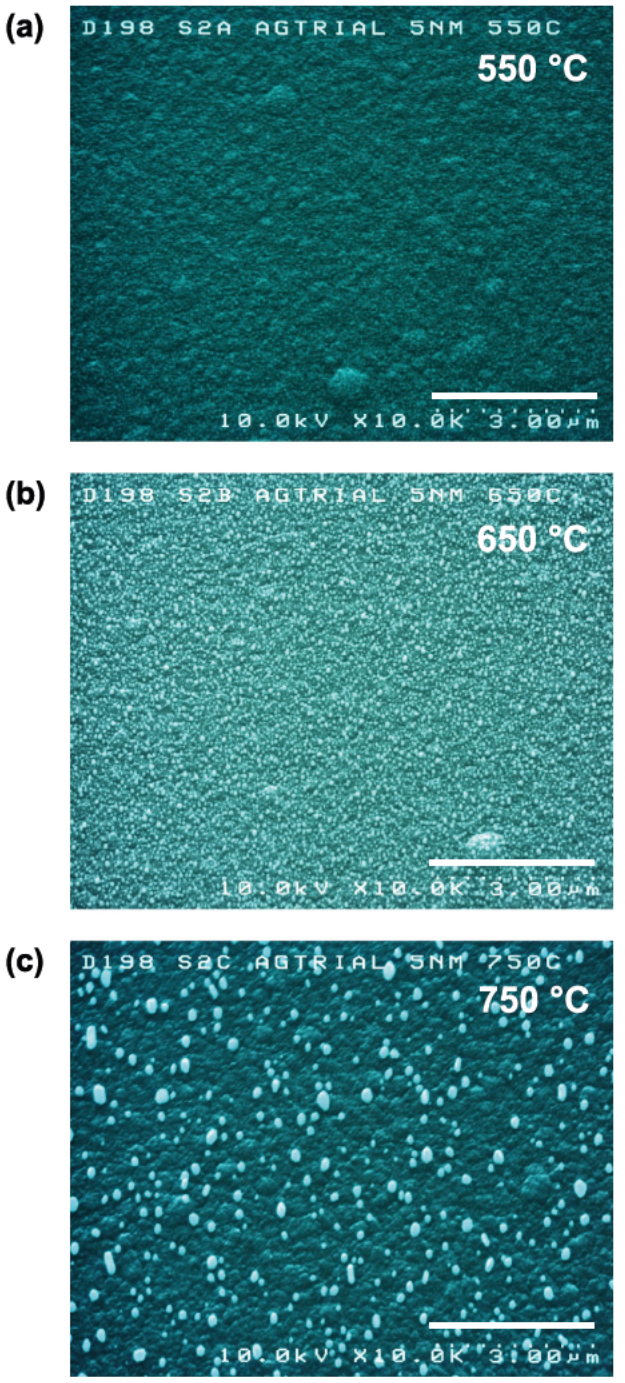

Fig. 4. SEM micrographs of silver nanodroplets obtained from a silver layer a with thickness of 5 nm after annealing at different temperatures (550 °C, 650 °C or 750 °C) (marker 3 µm).

nanodroplet size.

With these findings related to the mean size and distribution of the Ag nanodroplets we selected samples with an initial Ag layer thickness of 5 nm and a RTA treatment temperature of 650 °C for further ex periments.

3.3. *Embedding of silver nanodroplets in the UNCD films*

After a second UNCD capping deposition to enclose the surface silver nanodroplets, the composition of the final samples was in vestigated by AES. UNCD capping depositions with durations of 5 min, 10 min, 15 min and 30 min were performed and AES depth profiles were taken to reveal whether the Ag nanodroplets were completely embedded and how deep they were incorporated. The SEM observation of the FIB cuts of the samples prior the AES measurements could not show the incorporated nanodroplets. Furthermore, SEM micrographs taken from the surfaces after the capping depositions did not exhibit uncovered Ag nanodroplets irrespective of the capping duration (Fig. 6). The mean sputter rate with Ar ions was determined to be 2.5 nm/min applying the sputter parameters described above. For this purpose an as grown UNCD sample was entirely sputtered down to the Si substrate and the rate was calculeted assuming an average thickness of 220 nm. Considering the mean sputter rate the depth of the max imum silver content and the thickness of the layer with Ag were

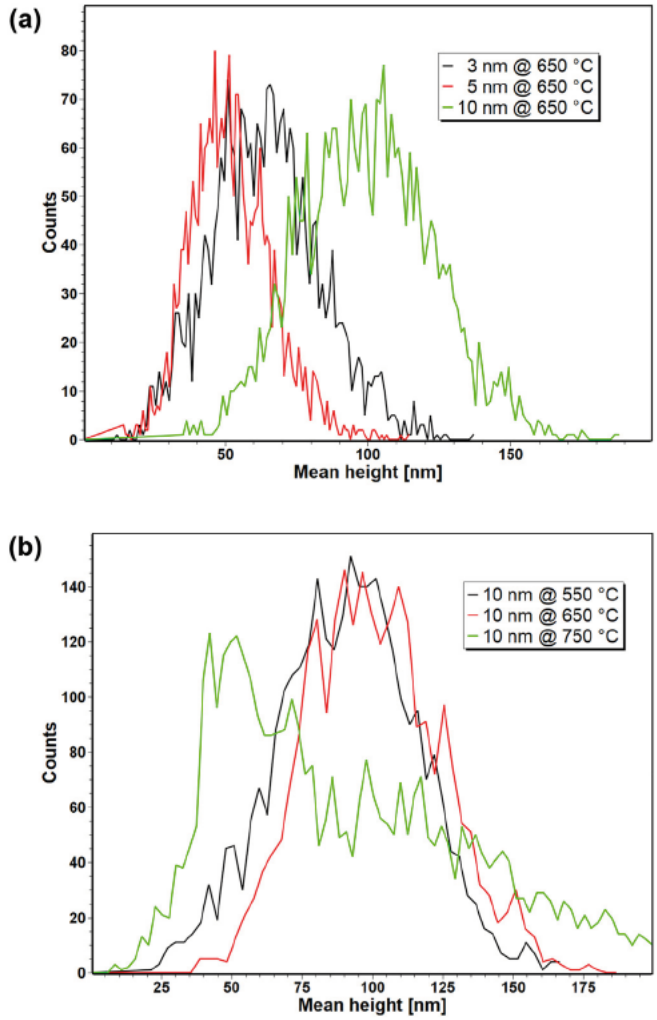

Fig. 5. Distribution of the mean height of the silver nanodroplets as a function of (a) silver layer thickness, (b) annealing temperature.

determined from the positions and widths of the peaks in Fig. 7 with an error margin of 5 nm since the sputter interval was 1 min.

From Fig. 7 it can be seen that after 5 min UNCD capping the silver content at the surface was 3.5 at.% as determined by AES. Since the information depth of the Auger electrons is within 1 2 nm it is possible that the Ag nanodroplets were very close to the surface covered with a very thin UNCD layer. In addition, Ag diffusion during the capping deposition with temperature around 600 °C should also be considered. After 5 min UNCD capping the highest silver signal was obtained di rectly from the surface, together with a second peak at a depth of 22.5 nm with a total thickness of around 42.5 nm. The 10 min and 15 min samples showed maximum silver concentrations at depths of 57.5 nm and 92.5 nm, respectively, with corresponding total thick nesses of around 52.5 nm and 50 nm. The thicknesses of the silver containg layers after UNCD capping for 5, 10 and 15 min were in good agreement with the result for the mean height of the silver nanodroplets (50 nm) derived from the AFM measurements. When discussing the depth profiles one should keep in mind that they could be influenced by some additional effects, such as knock on during sputtering and/or diffusion during the CVD overgrowth. The sample prepared with UNCD capping for 30 min showed some deviations from the trends observed for the other samples. The peak of silver was much broader, its max imum of 290 nm was deeper than expected and the thickness of around 102 nm higher compared to the other samples. This could be at least partially explained with increased growth rate after the initial stage of

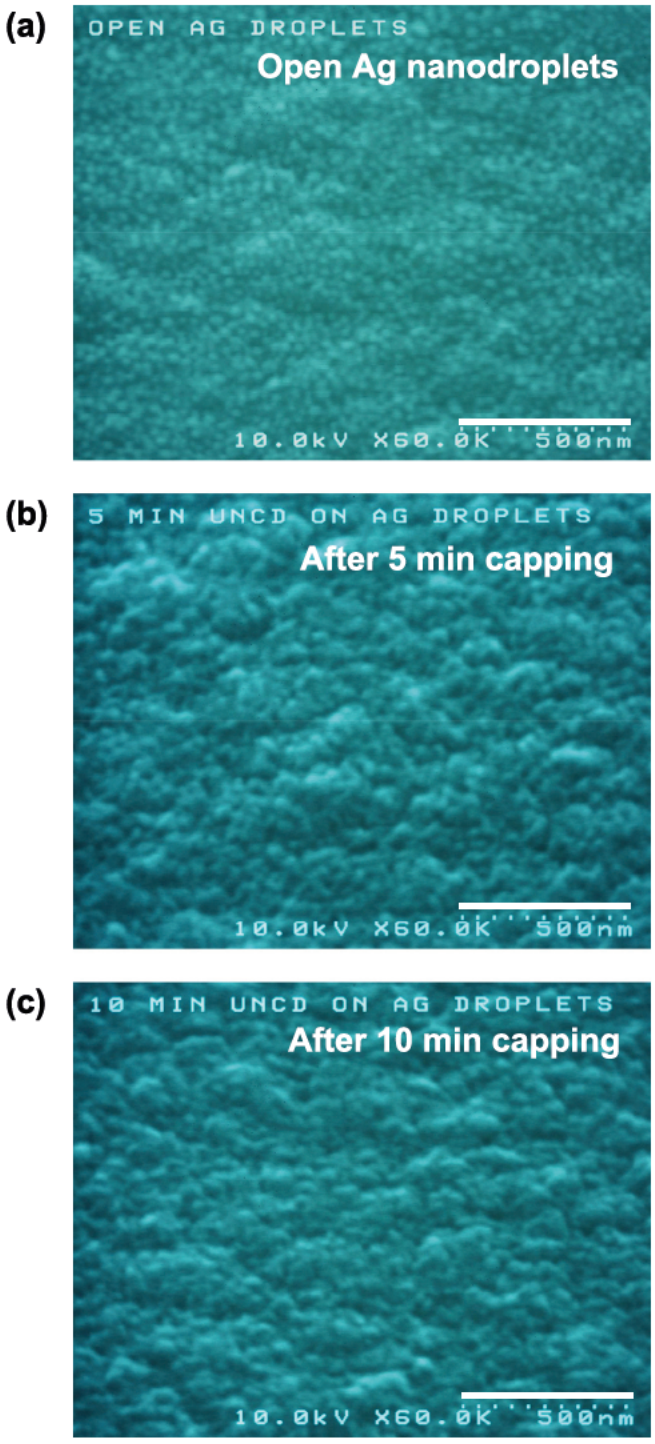

Fig. 6. SEM micrographs of samples with open Ag nanodroplets (a), after UNCD capping for 5 min (b) and 10 min (c) (marker 500 nm).

capping of the silver nanoparticles and some uncertainty by the de position of the silver layer. Nevertheless, this sample was also in vestigated by ICP MS in order to reveal the possiblity to utilize the capping layer thickness as a primary tool to control the amount of re leased silver.

3.4. Release of silver in aqueous samples

The samples for silver release experiments were prepared by sub merging 1 × 1 cm^2 UNCD/Ag/UNCD pieces in 20 ml deionized water

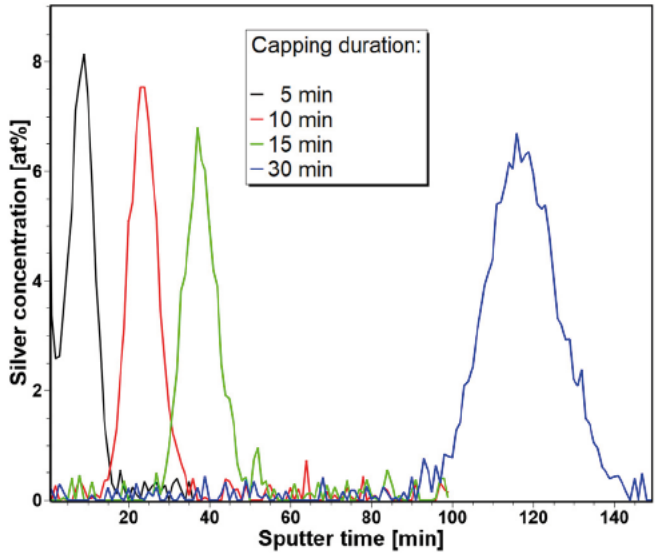

Fig. 7. Silver concentration depth profiles for UNCD/Ag/UNCD samples after 5, 10, 15 and 30 min UNCD capping deposition.

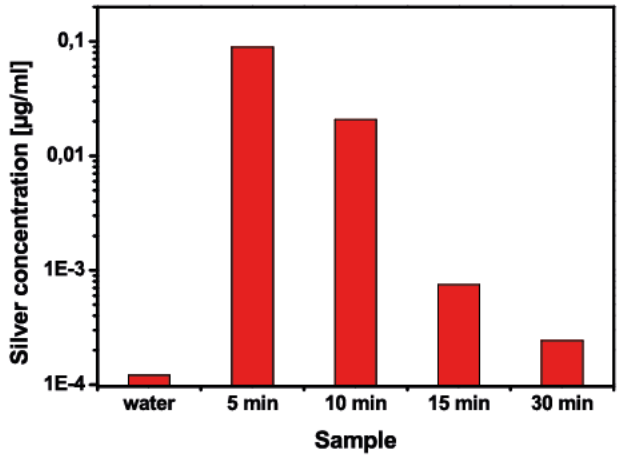

Fig. 8. Silver concentration in 20 ml deionized water after 7 days with submerged UNCD/Ag/UNCD samples with capping depositions of 5, 10, 15 and 30 min.

for 7 days at the physiological human body temperature of 37 °C. The aqueous samples were then examined by ICP MS with an additional sample of deionized water as a negative control and the results are shown in Fig. 8.

The results substantiate the idea of utilizing the UNCD capping layer to affect the amount of released silver: with increasing the capping layer thickness, the silver concentration in the aqueous samples decreased. The sample with 5 min UNCD capping showed the highest silver concentration of $(8.92 \pm 0.05) \times 10^{-2}$ µg/ml. It decreased to $(2.08 \pm 0.01) \times 10^{-2}$ µg/ml and $(7.48 \pm 0.02) \times 10^{-4}$ µg/ml for the samples with 10 and 15 min capping deposition, respectively. Even the sample with 30 min capping exhibited twice the silver concentration of the negative control which was significant considering the standard deviation of 2×10^{-6} µg/ml. Having in mind the AES results it was not surprising that the 5 min sample showed the highest silver concentration since the silver nanodroplets were not completely enclosed and remained partially in direct contact with the water. On the other hand, the detected Ag concentration in case of the 10 min sample was 170 times higher compared to the negative control clearly suggesting that there was migration of silver in the UNCD layer (possessing amorphous carbon matrix) because the layer was fully closed as seen from the AES results. This was also the case of the sample with 15 min capping but in much lesser extent (7 times increase) due to the thicker top UNCD layer. The pure mass of silver in the water was 1.78 µg, 0.42 µg and 0.014 µg for the samples with capping of 5, 10 and 15 min, respectively. Considering that approximately 5.25 µg of silver was deposited on each sample with 1×1 cm^2 surface area and 5 nm silver layer thickness (assuming a perfectly smooth surface which was not the case for the UNCD surfaces, i.e. the real surface area should be somewhat higher) it means that about 34% of the deposited silver was found in the water after 7 days for the 5 min sample and 8% for the 10 min sample. It is also worth mentioning that the size of the samples and therefore their active area was rather negligible compared to the water volume which made us confident for the bacterial assays although the bacterial inhibitory concentration of 0.3 µg/ml was not reached. For these tests samples with UNCD capping for 5 and 10 min were exploited.

3.5. Bacterial assay

The antibacterial properties of the UNCD/Ag/UNCD samples were determined by time kill tests. The time dependent antimicrobial effect was studied using the Gram positive bacterium *B. subtilis* and the Gram negative *E. coli*. The viability of the two bacterial strains, exposed to UNCD/Ag/UNCD samples with capping duration of 5 and 10 min, as well as samples with open silver nanodroplets (i.e. without capping deposition), as grown UNCD samples and pure bacterial culture, was evaluated after 3, 8 and 24 h. Equal aliquots of cells were spread over LB agar plates and the number of colony forming units (CFU) was counted after 24 h. The antibacterial efficiency (ABE) was calculated according to the formula:

$$\mathrm{ABE}\,(\%) = (N_{ref} - N_{exp})/N_{ref} \times 100$$

where N_{ref} is the number of bacterial colonies on the as grown UNCD control samples without Ag and N_{exp} their number on the experimental samples.

E. coli viability was not affected by the as grown surfaces where no silver was present, exhibiting similar growth after 3, 8 or 24 h exposure to the pure bacterial culture in accordance with the biocompatible properties of UNCD layers [46] (Fig. 9). The sample with surface silver nanodroplets was most toxic to the bacteria with the lowest CFU count from all samples after 3 h exposure and no growth at all after 8 h. The observed effect of the UNCD capping layer thickness on the antibacterial properties corroborated the results from the ICP MS regarding the release of silver. The bacterial growth was apparently reduced for the 5 min samples compared to the 10 min ones. This was the case after 3 h, even better expressed after 8 h and 24 h. After 24 h there was no growth visible for the 5 min samples in contrast to the 10 min ones. The determined antibacterial efficiency is presented in Fig. 10. Open silver nanoparticles were very toxic for the bacteria resulting in significant reduction of the number of living cells after 3 h and death of all bacteria after only 8 h of exposure. The partially coated 5 min samples revealed 70% reduction after 8 h and no living cells after 24 h. The 10 min sample with entirely enclosed silver nanodroplets could provide 80% reduction of bacteria after 24 h but it cannot be ruled out that this sample could also exhibit a bacteria free environment after longer period of exposure.

Exposure of the Gram positive *B. subtilis* to samples with open Ag nanodroplets and capped with UNCD for 5 min revealed excellent antibacterial properties already after 3 h reaching 100% lethality (Fig. 11). The bacterial growth was significantly reduced for the samples with 10 min capping after incubation for 3 and 8 h, and completely suppressed after 24 h (Fig. 12).

The UNCD/Ag/UNCD samples with 5 min capping deposition and the samples with open silver nanodroplets showed excellent antibacterial efficiency towards both bacterial species. The differences in the incubation period required to obtain a lethality percentage of 100% could be attributed to the different structures of the cell membranes.

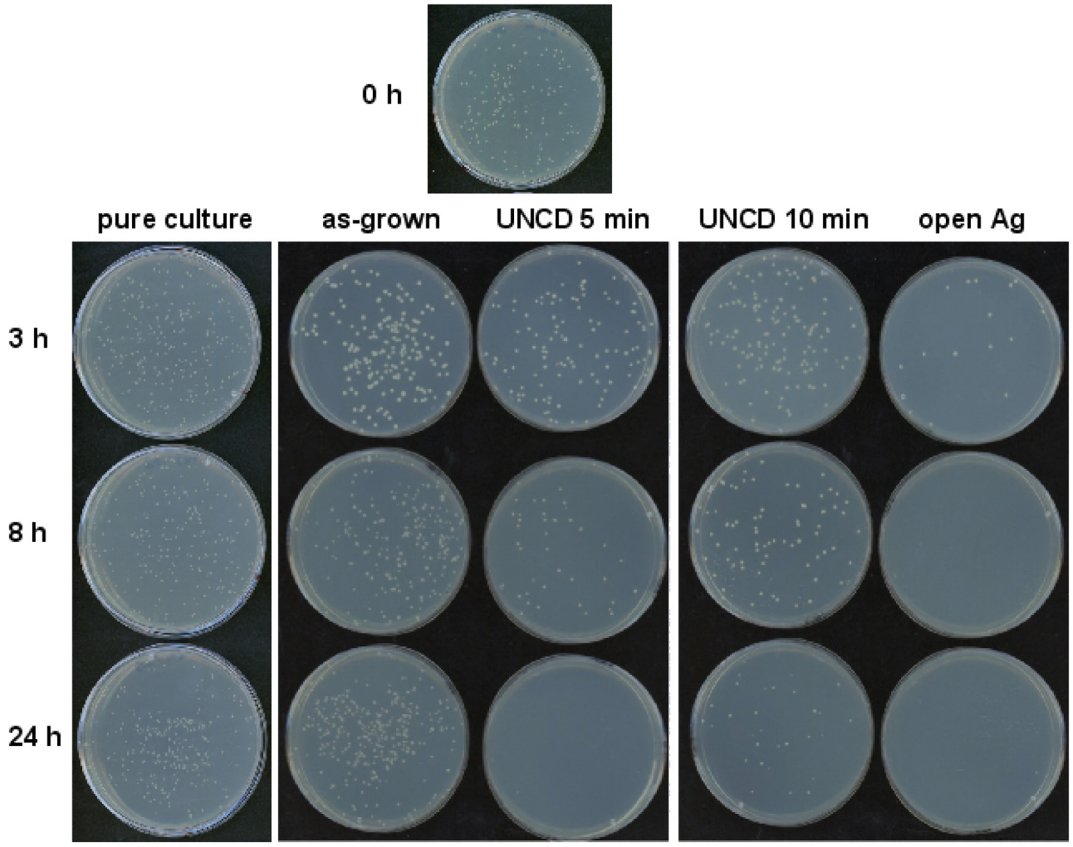

Fig. 9. Plates with *Escherichia coli* colonies representing the number of living cells after 3, 8 or 24 h exposure to UNCD/Ag/UNCD samples, samples with open silver nanodroplets and as-grown samples. Initial titer of the bacterial culture is presented (0 h). Pure bacterial culture was incubated in parallel as a control for biocompatability of the as-grown UNCD samples.

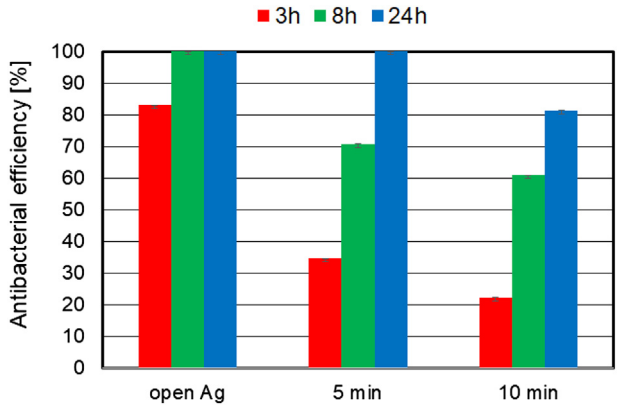

Fig. 10. Antibacterial efficiency against *Escherichia coli* after exposure for 3, 8 or 24 h to UNCD/Ag/UNCD samples and samples with open silver nanodroplets. Data represent the mean (± standard deviation) of three independent experiments.

The Gram negative *E. coli* possesses a thin peptidoglycan layer (about 2 3 nm) between the cytoplasmic membrane and the outer membrane, whereas the Gram positive *B. subtilis* lacks the outer membrane but has a peptidoglycan layer with thickness of ca. 30 nm [47,48]. This might affect the cell membrane disruption or direct uptake of silver during exposure, as well as the concentration necessary to achieve the desired antimicrobial effect.

In general, our results for the ABE of the UNCD/Ag/UNCD samples extend the family of carbon coatings incorporated with silver which can provide antimicrobial abilities when applied on implants or surgical tools. The direct comparison of the results regarding the ABE of the UNCD/Ag/UNCD samples with those of various Ag containing DLC coatings described above is difficult due to the different nature of the carbon materials and different silver content and distribution. In addition, the way the bacteria react to Ag exposure, for example in terms of transportation of Ag inside the bacteria and the ability to repair Ag induced damages, vary for different species or even different strains. However, some general trends can be highlighted. The thickness of the layer capping the Ag (irrespective of the capping material and the size of the silver particles) can be utilized to control the release of silver and therefore the effective ABE of the layer over a certain time span as reported in literature [30,36]. In addition, an optimized tests can be implemented to find the fine balance between the bactericidal abilities and the biocompatibility towards mammalian cells. At least for DLC Ag films some findings suggested an Ag concentration between 2 and 7 at. % as a good value to achieve this goal [32]. In contrast to the results in [30] we did not experience a saturation phenomenon like a decrease of the ABE after longer exposure times (3 h vs. 24 h) of the bacteria to the silver containing samples. In our case no recovery of the tested bacteria was apparent after a longer exposure period (up to 24 h). Also the trend whether Gram positive or Gram negative bacteria were more susceptible to the exposure to Ag containing coatings can not be generalized: in our case the Gram positive *B. subtilis* was more susceptible to the exposure to our UNCD/Ag/UNCD samples than the Gram negative *E. coli*, but for example, the Gram positive *S. aureus* was more persistent to DLC Ag exposure compared to the Gram negative *P. aeruginosa* [49]. On the other side, the time which was needed in the current study to achieve a (nearly) bacterial free environment was comparable with the times cited in literature [31,39,49].

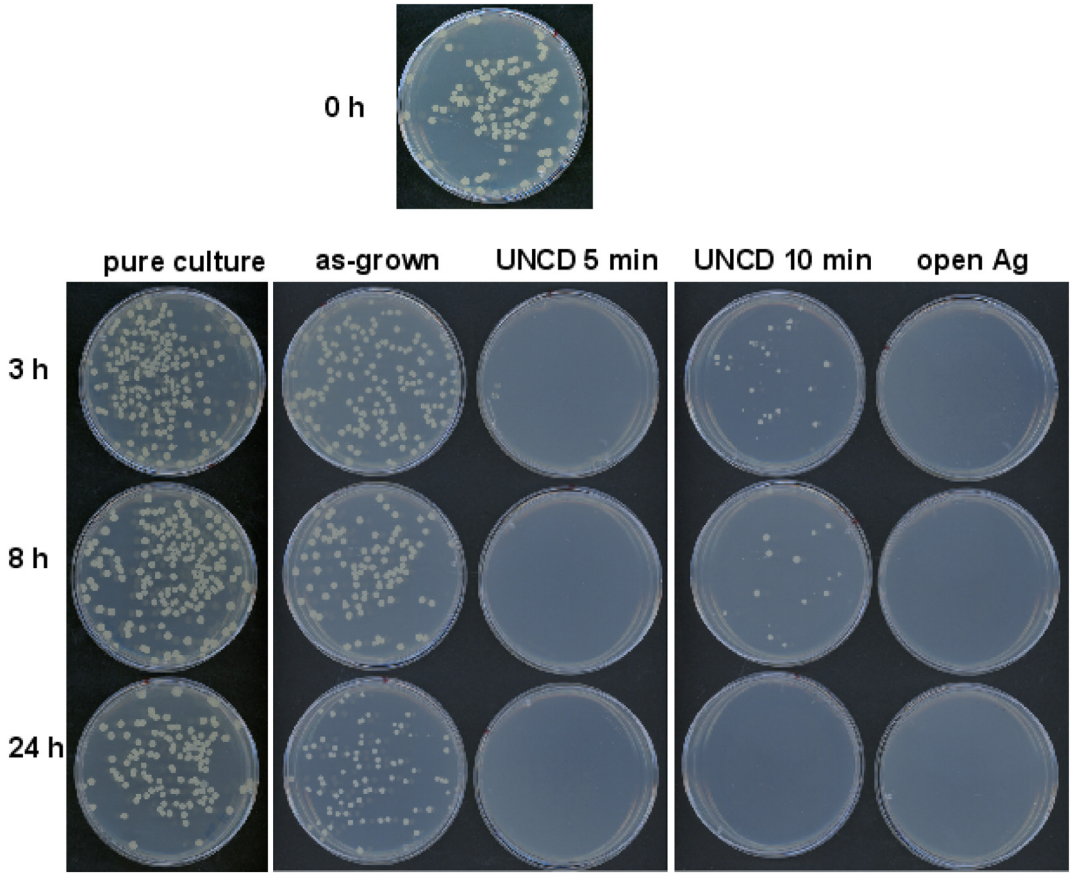

Fig. 11. Plates with *Bacillus subtilis* colonies after cell exposure for 3, 8 or 24 h to UNCD/Ag/UNCD samples, samples with open silver nanodroplets and as-grown samples. Initial titer of the bacterial culture is presented (0 h). Pure bacterial culture was incubated in parallel as a control for biocompatability of the as-grown UNCD samples.

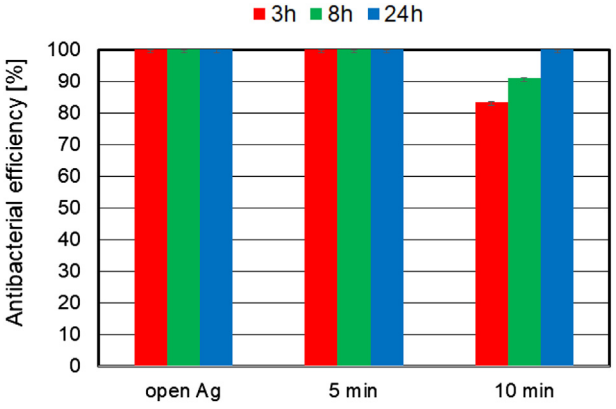

Fig. 12. Antibacterial efficiency against *Bacillus subtilis* after exposure for 3, 8 or 24 h to UNCD/Ag/UNCD samples and samples with open silver nanodroplets. Data represent the mean (± standard deviation) of three independent experiments.

4. Conclusions

In this work we provided ultrananocrystalline diamond films with antimicrobial abilities by embedding silver nanodroplets into the layer. After the deposition of the UNCD layers, the impact of the silver film thickness coated on top of it and the RTA treatment temperature on the silver nanodroplet morphology was investigated. SEM and AFM studies revealed that with increasing the layer thickness the size of the nanodroplets was also increasing and that an annealing temperature above 650 °C was causing loss of the desired uniformity resulting in nanodroplets with diverse shapes and sizes. For further experiments silver layer thickness of 5 nm and a RTA treatment temperature of 650 °C were selected due to the experienced good reproducebility of the nanodroplets regarding their average diameter of around 50 nm and their uniform distribution. In a following step a second UNCD deposition with duration between 5 and 30 min was performed for capping the silver nanodroplets targeting utilization of the thickness of the capping layer to control the amount of released silver. The AES study of the composition of the UNCD/Ag/UNCD samples revealed that the silver nanodroplets were completely covered after 10 min of UNCD capping deposition while after 5 min they are only partially coated. The release of silver from the samples into deionized water for 7 days was investigated by ICP MS. The results clearly indicated the effect of the capping layer thickness on the silver release. The partially covered 5 min sample showed the highest silver concentration with a 730 fold increase compared to the negative sample. Also the fully coated 10 and 15 min samples exhibited a 170 fold and a 7 fold increase, respectively which made it apparent that silver was migrating through the UNCD layer.

Finally, the antibacterial properties of UNCD/Ag/UNCD samples, as grown UNCD layers and UNCD samples with uncoated Ag nanodroplets were assessed directly with *E. coli* and *B. subtilis* as reference strains for Gram negative and Gram positive bacteria, respectively. The bacterial free environments obtained with the samples with surface Ag nanodroplets revealed the excellent antimicrobal effect of silver. The UNCD/Ag/UNCD samples also exhibited profound antibacterial propensity. The partially covered 5 min samples and the fully coated 10 min samples reduced the number of bacterial colonies after a given time span significantly and even erradicated all present bacteria. The 5 min samples reached a 100% antibacterial efficiency against *E. coli*

after 24 h and against *B. subtilis* after 3 h. In agreement with the AES and ICP MS results the ABE of the 10 min samples was lower due to the lower concentration of released silver. After 24 h the antibacterial efficiency against *E. coli* was 80% and 100% against *B. subtilis*.

The results clearly indicated the possibilty to provide the UNCD films, which are generally characterized with good mechanical properties, chemical inertness and sublime biocompatibility, also with supreme antibacterial propensity, increasing their attractiveness as implant coatings. Coated on implant materials, such as medical stainless steel, titanium or its alloys, UNCD/Ag/UNCD can provide the release of Ag ions to suppress the inflammatory processes in the first hours after surgery.

Acknowledgements

The authors would like to acknowledge the support of the Karlsruhe Nano Micro Facility (KNMF) which allowed us to use the equipment and the experience of the staff in an easy and uncomplicated manner. BP and GHB acknowledge funding by the Deutsche Forschungsgemeinschaft (DFG, German Research Foundation) within the SFB 860.

References

[1] J.S. Hayes, R.G. Richards, Expert Rev. Med. Devices 7 (2010) 843–853.
[2] W. Chen, S. Oh, A.P. Ong, N. Oh, Y. Liu, H.S. Courtney, M. Appleford, J.L. Ong, J. Biomed. Mater. Res. A 82 (2007) 899–906.
[3] P. Metzler, C. von Wilmowsky, B. Stadlinger, W. Zemann, K.A. Schlegel, S. Rosiwal, S. Rupprecht, J. Craniomaxillofac. Surg. 41 (2013) 532–538.
[4] S. Santavirta, Y.T. Konttinen, R. Lappalainen, A. Anttila, S.B. Goodman, M. Lind, L. Smith, M. Takagi, E. Gómez-Barrena, L. Nordsletten, J.-W. Xu, Curr. Orthop. 12 (1998) 51–57.
[5] D. Bociaga, K. Mitura, Diam. Relat. Mater. 17 (2008) 1410–1415.
[6] O. Auciello, A.V. Sumant, Diam. Relat. Mater. 19 (2010) 699–718.
[7] S.C.H. Kwok, W. Zhang, G.J. Wan, D.R. McKenzie, M.M.M. Bilek, P.K. Chu, Diam. Relat. Mater. 16 (2007) 1353–1360.
[8] J.E. Butler, Electrochem. Soc. Interface 12 (2003) 22–26.
[9] A. Carlisle John, O. Auciello, Electrochem. Soc. Interface 12 (2003) 28–31.
[10] L. Tang, C. Tsai, W.W. Gerberich, L. Kruckeberg, D.R. Kania, Biomaterials 16 (1995) 483–488.
[11] M.J. Papo, S.A. Catledge, Y.K. Vohra, C. Machado, J. Mater. Sci. Mater. Med. 15 (2004) 773–777.
[12] S. Rupprecht, A. Bloch-Birkholz, B. Lethaus, S. Rosiwal, F.W. Neukam, A. Schlegel, Clin. Oral Implants Res. 16 (2005) 98–104.
[13] G. Heinrich, B. Rinne, R. Thull, S.M. Rosiwal, R.F. Singer, Biomed Tech (Berl) (2009) 382–383.
[14] M.R. Hill, S.A. Catledge, V. Konovalov, W.C. Clem, S.A. Chowdhury, B.S. Etheridge, A. Stanishevsky, J.E. Lemons, Y.K. Vohra, A.W. Eberhardt, J Biomed Mater Res B Appl Biomater 85 (2008) 140–148.
[15] L. Yang, B.W. Sheldon, T.J. Webster, Biomaterials 30 (2009) 3458–3465.
[16] A.B.G. Lansdown, Silver in Healthcare: its Antimicrobial Efficacy and Safety in Use, (2010).
[17] J.F. Fisher, S.O. Meroueh, S. Mobashery, Chem. Rev. 105 (2005) 395–424.
[18] S.Y. Liau, D.C. Read, W.J. Pugh, J.R. Furr, A.D. Russell, Lett. Appl. Microbiol. 25 (1997) 279–283.
[19] W.J.A. Schreurs, H. Rosenberg, J. Bacteriol. 152 (1982) 7–13.
[20] W.K. Jung, H.C. Koo, K.W. Kim, S. Shin, S.H. Kim, Y.H. Park, Appl. Environ. Microbiol. 74 (2008) 2171–2178.
[21] J.J. Castellano, S.M. Shafii, F. Ko, G. Donate, Int. Wound J. 4 (2007) 139–140.
[22] H.-J. Park, J.Y. Kim, J. Kim, J.-H. Lee, J.-S. Hahn, M.B. Gu, J. Yoon, Water Res. 43 (2009) 1027–1032.
[23] J. Schierholz, J. Hosp. Infect. 40 (1998) 257–262.
[24] I. Chopra, J. Antimicrob. Chemother. 59 (2007) 587–590.
[25] B. Le Ouay, F. Stellacci, Nano Today 10 (2015) 339–354.
[26] A. Petica, S. Gavriliu, M. Lungu, N. Buruntea, C. Panzaru, Mater. Sci. Eng. B 152 (2008) 22–27.
[27] D.R. Monteiro, L.F. Gorup, A.S. Takamiya, A.C. Ruvollo-Filho, E.R. de Camargo, D.B. Barbosa, Int. J. Antimicrob. Agents 34 (2009) 103–110.
[28] L. Zhao, H. Wang, K. Huo, L. Cui, W. Zhang, H. Ni, Y. Zhang, Z. Wu, P.K. Chu, Biomaterials 32 (2011) 5706–5716.
[29] P. DeVasConCellos, S. Bose, H. Beyenal, A. Bandyopadhyay, L.G. Zirkle, Mater. Sci. Eng. C 32 (2012) 1112–1120.
[30] F.R. Marciano, L.F. Bonetti, L.V. Santos, N.S. Da-Silva, E.J. Corat, V.J. Trava-Airoldi, Diam. Relat. Mater. 18 (2009) 1010–1014.
[31] L.J. Wang, F. Zhang, A. Fong, K.M. Lai, P.W. Shum, Z.F. Zhou, Z.F. Gao, T. Fu, Thin Solid Films 650 (2018) 58–64.
[32] I.N. Mihailescu, D. Bociaga, G. Socol, G.E. Stan, M.C. Chifiriuc, C. Bleotu, M.A. Husanu, G. Popescu-Pelin, L. Duta, C.R. Luculescu, I. Negut, C. Hapenciuc, C. Besleaga, I. Zgura, F. Miculescu, Int. J. Pharm. 515 (2016) 592–606.
[33] C.A. Love, R.B. Cook, T.J. Harvey, P.A. Dearnley, R.J.K. Wood, Tribol. Int. 63 (2013) 141–150.
[34] M. Jelinek, T. Kocourek, J. Zemek, J. Mikšovský, Š. Kubinová, J. Remsa, J. Kopeček, K. Jurek, Mater. Sci. Eng. C 46 (2015) 381–386.
[35] L. Swiatek, A. Olejnik, J. Grabarczyk, A. Jedrzejczak, A. Sobczyk-Guzenda, M. Kaminska, W. Jakubowski, W. Szymanski, D. Bociaga, Diam. Relat. Mater. 67 (2016) 54–62.
[36] F.P. Schwarz, I. Hauser-Gerspach, T. Waltimo, B. Stritzker, Surf. Coat. Technol. 205 (2011) 4850–4854.
[37] D. Bociaga, P. Komorowski, D. Batory, W. Szymanski, A. Olejnik, K. Jastrzebski, W. Jakubowski, Appl. Surf. Sci. 355 (2015) 388–397.
[38] C. Gorzelanny, R. Kmeth, A. Obermeier, A.T. Bauer, N. Halter, K. Kümpel, M.F. Schneider, A. Wixforth, H. Gollwitzer, R. Burgkart, B. Stritzker, S.W. Schneider, Sci. Rep. 6 (2016) 22849.
[39] A. Mazare, A. Anghel, C. Surdu-Bob, G. Totea, I. Demetrescu, D. Ionita, Thin Solid Films 657 (2018) 16–23.
[40] G. Hazell, P.W. May, P. Taylor, A.H. Nobbs, C.C. Welch, B. Su, Biomater. Sci. 6 (2018) 1424–1432.
[41] A. Voss, H. Wei, Y. Zhang, S. Turner, G. Ceccone, J.P. Reithmaier, M. Stengl, C. Popov, Mater. Sci. Eng. C Mater. Biol. Appl. 64 (2016) 278–285.
[42] C. Popov, W. Kulisch, P.N. Gibson, G. Ceccone, M. Jelinek, Diam. Relat. Mater. 13 (2004) 1371–1376.
[43] C. Popov, W. Kulisch, S. Boycheva, K. Yamamoto, G. Ceccone, Y. Koga, Diam. Relat. Mater. 13 (2004) 2071–2075.
[44] W. Kulisch, T. Sasaki, F. Rossi, C. Popov, C. Sippel, D. Grambole, Phys. Status Solidi (RRL) 2 (2008) 77–79.
[45] W. Kulisch, C. Popov, E. Lefterova, S. Bliznakov, J.P. Reithmaier, F. Rossi, Diam. Relat. Mater. 19 (2010) 449–452.
[46] J. Miksovsky, A. Voss, R. Kozarova, T. Kocourek, P. Pisarik, G. Ceccone, W. Kulisch, M. Jelinek, M.D. Apostolova, J.P. Reithmaier, C. Popov, Appl. Surf. Sci. 297 (2014) 95–102.
[47] R.G. Murray, P. Steep, H.E. Elson, Can. J. Microbiol. 11 (1965) 547–560.
[48] G.D. Shockman, J.F. Barrett, Annu. Rev. Microbiol. 37 (1983) 501–527.
[49] P. Písařík, M. Jelínek, J. Remsa, J. Mikšovský, J. Zemek, K. Jurek, Š. Kubinová, J. Lukeš, J. Šepitka, Mater. Sci. Eng. C 77 (2017) 955–962.